Liquid Crystals
Publication details, including instructions for authors and subscription information:
http://www.informaworld.com/smpp/title~content=t713926090

A Comparison of the Molecular Dynamics of Fluorescent Probes in Curved Lipid Vesicles and Planar Multibilayers

Herman Van Langen[a]; Gijs Van Ginkel[a]; Yehudi K. Levine[a]
[a] Department of Molecular Biophysics, University of Utrecht, Utrecht, The Netherlands

To cite this Article Van Langen, Herman , Van Ginkel, Gijs and Levine, Yehudi K.(1988) 'A Comparison of the Molecular Dynamics of Fluorescent Probes in Curved Lipid Vesicles and Planar Multibilayers', Liquid Crystals, 3: 10, 1301 — 1317
To link to this Article: DOI: 10.1080/02678298808086612
URL: http://dx.doi.org/10.1080/02678298808086612

LIQUID CRYSTALS, 1988, VOL. 3, NO. 10, 1301–1317

A comparison of the molecular dynamics of fluorescent probes in curved lipid vesicles and planar multibilayers

by HERMAN VAN LANGEN, GIJS VAN GINKEL and YEHUDI K. LEVINE
Department of Molecular Biophysics, University of Utrecht, P.O. Box 80.000, 3508 TA Utrecht, The Netherlands

(*Received 1 March 1988; accepted 28 May 1988*)

The dynamic behaviour of the probe molecules DPH and TMA-DPH embedded in small unilamellar vesicles and planar multibilayers of POPC has been studied by time-resolved fluorescence depolarization techniques. The molecular dynamics of the probe molecules was analysed in terms of the rotational diffusion model. It is found that analysis of the time-dependent fluorescence anisotropy from the vesicle system yields two distinct, though statistically equivalent solutions. On the other hand the measurements on planar multibilayers can be interpreted unequivocally. It is shown that the order parameters of the probe molecules are higher in the multibilayers than in the vesicles. A reconstruction of the orientational distribution function reveals that the TMA-DPH molecules have a more pronounced tendency to lie with their long axes parallel to the bilayer surface in the curved vesicles than in the planar multibilayers. An intriguing finding is that the reorientational motion of the probes is considerably slower in the multibilayer samples than in the vesicles. These differences are attributed to the curvature and higher hydration of the bilayers in the vesicle systems.

1. Introduction

Fluorescent probes are widely used in studies of the molecular order and dynamics of natural and model membranes [1–3]. In particular the probes 1,6-diphenyl-1,3,5-hexatriene (DPH) and its more polar analogue 1-[4-(trimethylammonium)phenyl]-6-phenyl-1,3,5-hexatriene (TMA-DPH) are often chosen because of their favourable photophysical properties [2–5]. The dynamic behaviour of these molecules in many lipid systems can be adequately described by taking the molecules to possess cylindrical symmetry about their long axes [2, 3, 6–10]. As the absorption moments of the molecules lie parallel to the molecular symmetry axes, fluorescence depolarization experiments only sense the motion of the axes relative to the normal to the bilayer plane.

The main difficulty with fluorescence depolarization experiments is that the information about the order parameters

$$\langle P_2 \rangle = 1/2 \langle 3\cos^2 \beta - 1 \rangle$$

and

$$\langle P_4 \rangle = 1/8 \langle 35\cos^4 \beta - 30\cos^2 \beta + 3 \rangle$$

characterizing the orientational order and the diffusion coefficients or rotational correlation times describing the reorientational motions can only be obtained by fitting the experimental observations to a motional model [2, 3, 6–10]. It is important to realize, that this information can only be extracted from the experimental data if

the relative orientation of the absorption and emission moments is known. It is common practice, however, to assume that the two moments are parallel [2, 3, 5, 13].

Fluorescence depolarization experiments in the time domain are conveniently carried out on vesicle systems which possess an isotropic macroscopic symmetry. However, we have recently demonstrated [14] that the analysis of these experiments in terms of the rotational diffusion model is not unequivocal and indeed at least two sets of distinct model parameters yield equally good fits to the experimental data, as judged by statistical criteria. The question now arises as to which fit gives the physically more reasonable solution and how this can be tested. We have previously shown [6, 8–10, 15] that angle-resolved fluorescence depolarization experiments on oriented, planar, multibilayer systems afford the direct measurement of all the time correlation functions appearing in the theoretical description of the experiments, whereas only their sum can be obtained from anisotropy experiments on macroscopically isotropic vesicle systems [2, 12, 14]. Indeed dynamic information can be obtained from angle-resolved experiments under conditions of continuous illumination, provided the intrinsic fluorescence decay of the probe molecules is known [9, 10, 16, 17]. We shall show here that time- and angle-resolved fluorescence depolarization experiments on multibilayer samples allow the resolution of the ambiguity encountered in the analysis of the experiments on lipid vesicles.

We report further the analyses of fluorescence depolarization experiments on TMA-DPH molecules embedded in small unilamellar vesicles and in oriented multibilayers of palmitoyloleoyl phosphatidylcholine (POPC) in terms of the rotational diffusion model. Some problems underlying the description of the vesicle data are discussed and the methodology of the experiments on oriented samples is tested using solutions of DPH molecules in paraffin oil. We show that TMA-DPH molecules have a greater propensity to lie parallel to the bilayer surface in vesicles than in the multibilayer samples. An intriguing finding is that the motion of the probe is considerably faster in vesicles than in multibilayer systems. These differences are attributed to the effects of the curvature and hydration of the lipid bilayers on the behaviour of the probe molecules.

2. Theory

2.1. *Theoretical expressions*

The theory of fluorescence depolarization experiments in membrane systems has been discussed in detail by Johansson and Lindblom [18], van der Meer *et al.* [15] and Zannoni *et al.* [2] and will only be summarized here. We shall consider an idealized experiment in which the fluorophores are excited by an instantaneous light pulse at time $t = 0$ and the fluorescence emission is observed at time t. The absorption and emission processes are characterized by the transition dipole moments $\boldsymbol{\mu}$ and $\boldsymbol{\nu}$ respectively and is assumed to be independent. The decay of the excited state is taken to be a random process, characterized by an isotropic, normalized, probability function $F(t)$ and the depolarization process is assumed to be entirely due to the reorientational motion of the fluorescent molecule. In particular we discuss the experimental arrangement depicted in figure 1, for studying slab-shaped membrane samples. The plane of the sample is vertical and the XY plane is horizontal; the sample can be rotated about the vertical Z axis. A δ function pulse of plane polarized light with the electric vector along $\mathbf{e}_i$ is incident along the X axis, and the fluorescence emission scattered at an angle ψ relative to the negative X axis, with its electric field

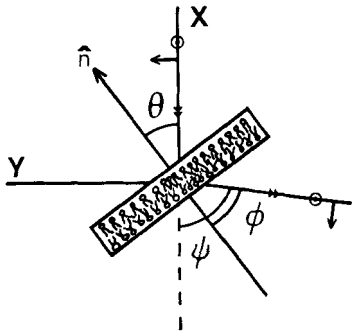

Figure 1. The experimental geometry for angle-resolved fluorescence depolarization measurements on slab-shaped samples. The XY plane is horizontal and the sample plane vertical.

polarized along $\mathbf{e}_f$ is detected. The angles θ and ϕ shown in figure 1 are, respectively, the angle of incidence and observation relative to the normal to the sample surface and furthermore $\psi = \theta + \phi$. The angles are taken to be positive in the configuration shown, but change sign as either beam moves to the other side of the normal. We note here that the two eigenmodes for the sample are polarizations along the Z axis and in the XY plane. The fluorescence intensity is given by

$$I_{if}(t) = k\langle(\mathbf{e}_i \cdot \boldsymbol{\mu})^2(\mathbf{e}_f \cdot \boldsymbol{\nu})^2\rangle F(t), \tag{1}$$

where k contains fundamental constants and depends on the concentration of the fluorophores and the illuminated volume. Equation (1) can be separated into independent factors describing the experimental geometry and the molecular properties of the fluorophores in the sample by making use of the second rank Legendre polynomial

$$P_2(\cos\theta) = 1/2(3\cos^2\theta - 1)$$

and the closure relation for Wigner rotation matrices [2, 19, 21]

$$\begin{aligned} I_{if}(t) = k/9 \langle 1 &+ 2P_2[\cos(\mathbf{e}_i \cdot \boldsymbol{\mu})] + 2P_2[\cos(\mathbf{e}_f \cdot \boldsymbol{\nu})] \\ &+ 4P_2[\cos(\mathbf{e}_i \cdot \boldsymbol{\mu})]P_2[\cos(\mathbf{e}_f \cdot \boldsymbol{\nu})]\rangle F(t), \end{aligned} \tag{2}$$

where

$$P_2[\cos(\mathbf{e}_i \cdot \boldsymbol{\mu})] = \sum_{jk} D^2_{j0}{}^*(\phi_i\theta_i 0)D^2_{jk}(\Omega_{ls})D^2_{k0}(\alpha_\mu\beta_\mu 0) \tag{3a}$$

and

$$P_2[\cos(\mathbf{e}_f \cdot \boldsymbol{\nu})] = \sum_{mn} D^2_{m0}(\phi_f\theta_f 0)D^2_{mn}{}^*(\Omega_{ls})D^2_{n0}{}^*(\alpha_\nu\beta_\nu 0). \tag{3b}$$

Here ϕ and θ denote the azimuthal and polar angles of $\mathbf{e}_i$ and $\mathbf{e}_f$ in the laboratory frame, Ω_{ls} are the Euler angles [19] describing the orientation of the sample in the laboratory frame and $(\alpha\beta 0)$ denotes the orientation of $\boldsymbol{\mu}$ at time $t = 0$ and of $\boldsymbol{\nu}$ at time t in the sample frame.

We can make use of four combinations of the polarization directions of the excitation and emission beams: VV, VH, HV and HH, where V denotes polarization along the Z axis, and H polarization in the XY plane but perpendicular to the direction of propagation of the light beam. Note that the first letter gives the polarization direction of the excitation beam. The corresponding orientations of $\mathbf{e}_i$ and $\mathbf{e}_f$ are given in table 1.

Table 1. Angles of the polarization directions of excitation and emission light.

	ϕ_i	θ_i	ϕ_f	θ_f
VV	0	0	0	0
VH	0	0	$\pi/2 + \psi$	$\pi/2$
HV	$\pi/2$	$\pi/2$	0	0
HH	$\pi/2$	$\pi/2$	$\pi/2 + \psi$	$\pi/2$

Note: $\psi = \theta + \phi$, where θ is the angle of incidence and ϕ is the angle of observation defined within the sample.

For the sake of brevity we shall henceforth use the definitions

$$\left.\begin{aligned} S_\mu &= \langle P_2(\cos\beta_\mu)\rangle, \\ S_\nu &= \langle P_2(\cos\beta_\nu)\rangle, \\ G_k(t) &= \langle D^2_{k0}(\alpha_\mu\beta_\mu 0)D^{2*}_{k0}(\alpha_\nu\beta_\nu 0)\rangle \quad k = 0, 1, 2. \end{aligned}\right\} \tag{4}$$

It is important to note further that in the uniaxial membrane systems considered here [20] $G_k(t) = G_{-k}(t)$ and [21]

$$\langle D^2_{k0}(\alpha_\mu\beta_\mu 0)D^{2*}_{j0}(\alpha_\nu\beta_\nu 0)\rangle = G_k(t)\delta_{jk}.$$

On making use of equations (2)–(4), together with the angles given in table 1, we can evaluate the intensities observed in experiments utilizing the configuration shown in figure 1 for which $\Omega_{ls} = \{\theta\pi/20\}$. After some lengthy, but straightforward calculations making use of the explicit expressions for the Wigner rotation matrix elements [21] we obtain

$$9I_{VV}(t)/kF(t) = 1 - S_\mu - S_\nu + G_0(t) + 3G_2(t), \tag{5a}$$

$$9I_{VH}(t)/kF(t) = 1 - S_\mu - S_\nu(1 - 3\sin^2\phi) + G_0(t)(1 - 3\sin^2\phi) - 3G_2(t)(1 - \sin^2\phi), \tag{5b}$$

$$9I_{HV}(t)/kF(t) = 1 - S_\nu - S_\mu(1 - 3\sin^2\theta) + G_0(t)(1 - 3\sin^2\theta) - 3G_2(t)(1 - \sin^2\theta), \tag{5c}$$

$$9I_{HH}(t)/kF(t) = 1 - S_\nu(1 - 3\sin^2\phi) - S_\mu(1 - 3\sin^2\theta) + G_0(t)(1 - 3\sin^2\phi)(1 - 3\sin^2\theta) - 3G_1(t)\sin 2\phi \sin 2\theta + 3G_2(t)(1 - \sin^2\phi)(1 - \sin^2\theta). \tag{5d}$$

It can be seen from equations (5) that two parameters S_μ, S_ν and three correlation functions $G_0(t)$, $G_1(t)$ and $G_2(t)$ describe the polarized intensities. In principle they can all be obtained from time-resolved experiments on a single sample geometry by a simultaneous analysis of the time behaviour of the four intensities. It is important to realize, however, that the correlation function $G_1(t)$ does not contribute to the observed intensities for those experiments with either $\theta = 0$ or $\phi = 0$, i.e. normal incidence or observation. We stress here that the effects of refraction at the sample/air interface have been neglected in the derivation of equations (5).

2.2. *Application to DPH and TMA-DPH molecules*

DPH and TMA-DPH molecules may be considered to behave as cylindrically symmetric objects with their absorption transition moments lying parallel to the long

molecular axes ($\beta_\mu = 0$). We shall furthermore take the emission moment to be tilted by an angle β_ν relative to the long axis. This assumption is based on our findings from studies using continuous illumination conditions that the order parameter of the absorption transition moment is significantly higher than that of the emission moment [6, 8–10, 16, 17]. We can now interpret the experimental quantifies S_μ, S_ν, G_0, G_1 and G_2 in terms of the orientational behaviour of the molecules by carrying out the successive rotational transformations: sample frame → molecular frame → transition moment frame [2, 19]. Let ($\alpha\beta 0$) now denote the direction of the transition moment in the molecule fixed frame and Ω_{sm} the orientation of the molecule in the sample, so that we have

$$\begin{aligned} S_\mu &= \left\langle \sum_j D^2_{0j}(\Omega_{sm}) D^2_{j0}(\alpha_\mu \beta_\mu 0) \right\rangle \\ &= \langle P_2 \rangle, \end{aligned} \tag{6a}$$

$$\begin{aligned} S_\nu &= \left\langle \sum_k D^2_{0k}(\Omega_{sm}) D^2_{k0}(\alpha_\nu \beta_\nu 0) \right\rangle \\ &= \langle P_2 \rangle P_2(\cos \beta_\nu). \end{aligned} \tag{6b}$$

Here we have made use of the fact [21] that $\langle D^L_{0j}(\Omega_{sm}) \rangle = \langle D^L_{00}(\Omega_{sm}) \rangle \delta_{j0} = \langle P_L \rangle$ for cylindrically symmetric molecules. P_L denotes the Legendre polynomial of order L. In a similar way we find

$$\begin{aligned} G_k(t) &= \sum_{nm} \langle D^2_{kn}(\Omega_{sm}(0)) D^{2*}_{km}(\Omega_{sm}(t)) \rangle D^2_{n0}(\alpha_\mu \beta_\mu 0) D^{2*}_{m0}(\alpha_\nu \beta_\nu 0) \\ &= P_2(\cos \beta_\nu) \langle D^2_{k0}(\Omega_{sm}(0)) D^{2*}_{k0}(\Omega_{sm}(t)) \rangle \end{aligned} \tag{7}$$

since for cylindrically symmetric molecules we have [20, 21]

$$\langle D^2_{kn}(\Omega_{sm}(0)) D^{2*}_{km}(\Omega_{sm}(t)) \rangle = \langle D^2_{kn}(\Omega_{sm}(0)) D^{2*}_{kn}(\Omega_{sm}(t)) \rangle \delta_{mn}.$$

Note that $\Omega_{sm}(t)$ denotes the molecular orientation at time t.

The evaluation of the time behaviour of the correlation functions $G_k(t)$ as a result of reorientational motions is cumbersome and in fact only possible in terms of physical models for the molecular motion [2, 7, 20]. Nevertheless, since the motion can be described as a stochastic process, the values of $G_k(t)$ for $t = 0$ and $t \to \infty$ are model independent. The $G_k(0)$ can be expressed in terms of linear combinations of the molecular order parameters $\langle P_2 \rangle$ and $\langle P_4 \rangle$. In the latter limit we have

$$\begin{aligned} G_k(\infty) &= P_2(\cos \beta_\nu) \langle D^2_{k0}(\Omega_{sm}(0)) \rangle \langle D^{2*}_{k0}(\Omega_{sm}(\infty)) \rangle \\ &= P_2(\cos \beta_\nu) \langle P_2 \rangle^2 \delta_{k0}, \end{aligned} \tag{8}$$

where the second equality expresses the uniaxial symmetry of the membrane sample. It is important to realize that $\langle P_2 \rangle$ can thus be obtained in a straightforward way from the plateau reached by $G_0(t)$ at long times.

We now consider the time behaviour of $G_{k(t)}$ for molecules undergoing a small step rotational diffusion subject to the orienting potential $U(\beta_{sm})$ [2, 20]

$$U(\beta_{sm}) = -kT\{\lambda_2 P_2(\cos \beta_{sm}) + \lambda_4 P_4(\cos \beta_{sm})\}. \tag{9}$$

The choice of this potential is based on the following consideration. We have seen above that only the two order parameters $\langle P_2 \rangle$ and $\langle P_4 \rangle$ are accessible experimentally in a model independent way. As equation (9) represents the simplest potential spanning all the physically permissible pairs of ($\langle P_2 \rangle$, $\langle P_4 \rangle$), we have no *a priori*

reason to include other terms. This conclusion can also be reached on the basis of the maximum entropy method [22]. We note that the orientational distribution function of the molecules is given by

$$f(\beta_{sm}) = N \exp\{-U(\beta_{sm})/kT\}$$

with N a normalizing constant. The time dependence of the correlation functions is obtained from a numerical solution of the diffusion equation [2, 20] and can be shown to be given as an infinite sum of exponential decays

$$G_k(t) = P_2(\cos\beta_v) \sum_{m=0}^{\infty} b_m^k \exp(-D_\perp \alpha_m^k t), \tag{10}$$

where the amplitudes b_m^k and the exponential factors α_m^k are determined by λ_2 and λ_4 (and hence $\langle P_2 \rangle$ and $\langle P_4 \rangle$). $D_\perp$ is the diffusion coefficient of the long molecular axis. In many practical situations, the correlation functions are found to have a mono-exponential decay of the form

$$G_k(t) = \{G_k(0) - G_k(\infty)\} \exp(-\alpha^k D_\perp t) + G_k(\infty). \tag{11}$$

Useful approximations for α_k in terms of $\langle P_2 \rangle$ and $\langle P_4 \rangle$ have been given by van der Meer *et al.* [23].

2.3. *Lipid vesicles*

Suspensions of lipid vesicles can be considered as an ensemble of the slab-shaped samples discussed previously, but with the normals to the planes having random orientations in the sample frame, i.e. complete orientational disorder [2]. In this case the transition moments are also randomly distributed so that their order parameters S_μ and S_v (cf. equation (4)) are identically zero. In order to evaluate the correlation functions $G_k(t)$, we now resolve the rotational transformation, sample frame → molecule frame into the successive transformations sample frame → slab frame → molecular frame and average over all the orientations of the slabs [2]

$$G_k(t) = P_2(\cos\beta_v) \sum_{mn} \langle D_{km}^2(\Omega_{sd}) D_{kn}^{2*}(\Omega_{sd}) \rangle \langle D_{m0}^2(\Omega_{dm}(0)) D_{n0}^{2*}(\Omega_{dm}(t)) \rangle, \tag{12}$$

where Ω_{sd} and Ω_{dm} are respectively the orientations of the slab in the sample frame and of the molecule in the slab frame. We note that Ω_{dm} in equation (12) is formally equivalent to Ω_{sm} in equations (7) and (8). We have here furthermore recognized that the molecular behaviour in the slab is independent of the macroscopic orientation of the slab [2]. On noting that

$$\langle D_{km}^2(\Omega_{sd}) D_{kn}^{2*}(\Omega_{sd}) \rangle = (1/5)\delta_{mn}$$

equation (12) reduces to

$$G_k(t) = (1/5) P_2(\cos\beta_v) \sum_{m} \langle D_{m0}^2(\Omega_{dm}(0)) D_{m0}^{2*}(\Omega_{dm}(t)) \rangle \tag{13}$$

so that $G_k(t)$ is independent of the index k. Thus $G_0(t) = G_1(t) = G_2(t)$ and is given by a sum of correlation functions for the motions of the molecules. These functions are identical to those appearing in equation (7). It is now easy to show that the time-dependent anisotropy $r(t)$ is given by

$$r(t) = (2/5)\{G_0(t) + 2G_1(t) + 2G_2(t)\}, \tag{14}$$

where $G_k(t)$ is given by equation (7). In the limiting case of complete orientational disorder within the bilayer, equation (14) reduces to the usual form

$$r(t) = (2/5)P_2(\cos\beta_v)\exp(-6D_\perp t). \quad (15)$$

3. Experimental

3.1. *Sample preparation*

The probe molecules DPH and TMA-DPH were purchased respectively from Fluka AG and Molecular Probes Inc. and used as received. Fresh stocks of the probes in ethanol (5×10^{-4} M) were kept in darkness at 4°C. POPC was purchased from Sigma Chemical Co. and used without further purification. The lipid was dissolved in a mixture of ethanol and freshly, doubly distilled chloroform. Solutions of the probe molecules were added as necessary to give a lipid: probe molecular ratio of 250 : 1. The solvent was then removed by evaporation under nitrogen gas followed by exposure to high vacuum for 12 h.

3.1.1. *Multibilayer preparation*

The dried lipid/probe mixture was allowed to equilibrate with water vapour above a saturated solution of K_2SO_4 (96 per cent relative humidity) for 24 h under a nitrogen atmosphere. Macroscopically oriented multibilayers were prepared by gently rubbing the hydrated lipid mixture between two microscope glass coverslips. The alignment was carried out at room temperature (22°C) and monitored by a polarizing microscope equipped with a first-order red plate. After alignment the samples were reequilibrated with water vapour and sealed along their edges with two-component epoxy resin to prevent dehydration. The contribution of scattered excitation to fluorescence light was minimized by completely blackening the samples except for a circular area 4 mm in diameter. All the preparative steps were carried out in the dark, as much as possible.

3.1.2. *Vesicle preparation*

The dried lipid/probe mixture was dispersed in 6 ml of a buffer containing 2×10^{-2} M Tris and $7{\cdot}5 \times 10^{-6}$ M EDTA at pH 8·0. Vesicles were formed by sonicating the aqueous dispersion in the dark under a nitrogen atmosphere in a bath type sonicator. Any large liposome remnants were removed by centrifuging for 1 h at 150·000 g. The final vesicle suspensions contained $1{\cdot}3 \pm 0{\cdot}2$ mg lipid/ml buffer solution determined by phosphorus analysis [26].

3.2. *Experimental setup*

The sample holder and PM tube housing were mounted on two goniometers having a common vertical axis and the angles θ and ϕ could be set to within 1°. Measurements on vesicles were carried out with the conventional 90°-scattering geometry. Angle-resolved measurements on slab-shaped samples were carried out with normal incidence ($\theta = 0$) of the horizontally polarized exciting light. The fluorescence intensities $I_{HV}(t)$ and $I_{HH}(t)$ were measured for four different detection angles, $\phi = 20°$, 30°, 40° and 50°, set in air outside the sample. The probe molecules were excited by a parallel beam of plane-polarized light (358 ± 5 nm, Spex monochromator). The fluorescence emission was passed through a GG 395 low cut-off

filter (Schott) and a Balzers interference filter, 438 ± 7 nm, before incidence on the PMT (Philips, XP2020Q). A standard single-photon counting system was used for detection [11]. The temperature during the experiments was 20°C.

3.3. *Time-resolved measurements*

The time-resolved measurements were carried out with the synchrotron radiation source (SRS) in Daresbury, UK, operating in the single-bunch mode. The start pulse was obtained from a ring pulse generated by the circulating 2 GeV electrons. The first photon detected by the PMT provided the stop pulse for the time-to-pulse-height converter (TPHC, Ortec 457). The output pulses from the TPHC were digitized and stored in a multichannel analyser (MCA, INO-TEC 5400) using 1024 channels for each recorded signal. The excitation functions were obtained from elastic scattering by the samples at the emission wavelength. In all the experiments the count rates were kept below 1 per cent of the excitation pulse repetition rate in order to avoid problems due to pile-up.

3.4. *Optical corrections*

The experimental data must be corrected in order to take into account the differential sensitivity of the PMT to the state of polarization of the light and the refraction at the sample/air interfaces. The PMT correction factor was determined by measuring the polarization ratio of the fluorescence emission from a DPH solution in ethanol, where complete depolarization is expected. A 90°-scattering geometry was used. The factor was found to be 1·004 ± 0·004. The refractive index of the lipid samples was taken as 1·5. No corrections for transmission losses at the sample/air interfaces were necessary.

3.5. *Numerical analysis*

Non-linear least squares reiterative deconvolution methods [11] were used in the analysis of the experimental decay curves. The least-squares optimization was carried out with the ZXSSQ routine from the IMSL library. All the measured decay curves were analysed simultaneously. Equations (5 *a*), (5 *b*) and (13) were used in the analysis of the vesicle data on setting $\phi = \pi/2$ and $S_\mu = S_v = 0$. The decays observed from the oriented samples were analysed using equations (5 *c*) and (5 *d*). Only channels between 150 to 750 (TMA-DPH) or 150 to 1024 (DPH) were used for the optimization of the parameters.

4. Results and discussion

4.1. *TMA-DPH in POPC vesicles*

The two decay curves $I_{VH}(t)$ and $I_{VV}(t)$ obtained from a 90°-scattering geometry were analysed using the rotational diffusion model on taking the intrinsic fluorescence decay $F(t)$ of the TMA-DPH molecules to have a normalized biexponential form

$$F(t) = (\beta_1/\tau_{F1})\exp(-t/\tau_{F1}) + (\beta_2/\tau_{F2})\exp(-t/\tau_{F2}). \quad (16)$$

In addition the factor $P_2(\cos\beta_v)$ was taken to be an adjustable parameter. Thus the optimization of eight parameters, four each for the anisotropy decay and the fluorescence decay, is required in the numerical deconvolution procedure. The simultaneous analysis of the decay curves revealed, however, two distinct, but statistically

Table 2. Recovered fit parameters for the two χ_r^2 minima for TMA-DPH molecules in POPC vesicles.

Minimum	χ_r^2	β_1	τ_{F1} ns	β_2	τ_{F2} ns	$P_2(\cos\beta_v)$	$\langle P_2\rangle$	$\langle P_4\rangle$	$D_\perp$ ns^{-1}
I	1·464	0·36	1·40	0·64	4·45	0·81	0·51	0·42	0·089
Errors		0·005	0·02	0·005	0·03	0·03	0·03	0·02	0·007
II	1·469	0·35	1·36	0·65	4·43	0·78	0·56	0·01	0·072
Errors		0·005	0·02	0·005	0·03	0·03	0·10	0·12	0·024

equivalent, solutions. The minimum located by the numerical deconvolution procedure was found to be dependent on the values assigned to the four parameters $P_2(\cos\beta_v)$, $\langle P_2\rangle$, $\langle P_4\rangle$ and $D_\perp$ describing the time-correlation functions at the start of the search. The model parameters for the two solutions are summarized in table 2. It can be seen from the table that both solutions yield virtually the same fluorescence decay, but significantly different order parameters and diffusion coefficients. In fact solution II appears to yield similar order parameters to those expected from the wobble-in-cone model [3]. The small differences in $\langle P_2\rangle$ for the two minima arise simply because the weighted least squares procedure conserves the area under the measured curve [24] so that equations (5*a*) and (5*b*) require that

$$\int_0^\infty F(t)r(t)dt$$

is an experimental constant. We note that the recovered value of $P_2(\cos\beta_v)$ is in good agreement with that obtained by us earlier from steady state angle resolved measurements on POPC multibilayers [9, 17]. Indeed the values of the other model parameters found by us from the latter experiments are similar to those obtained for solution I for the vesicle data.

In order to check the recovered value of $P_2(\cos\beta_v)$ we have carried out a global fit of the data describing the anisotropy $r(t)$ as a biexponential decay with a limiting term $r(\infty)$. This analysis yielded $r(0) = 0{\cdot}314$ and $r(\infty) = 0{\cdot}092$, corresponding to $\langle P_2\rangle = 0{\cdot}54$ and $P_2(\cos\beta_v) = 0{\cdot}785$, in good agreement with the values found for solution II.

In view of the fact that the values of $P_2(\cos\beta_v)$ recovered in the analysis were significantly lower than unity ($\beta_v = 0$), we have analysed the data systematically by keeping this parameter constant during the deconvolution procedures and considered solution I only. In these calculations $P_2(\cos\beta_v)$ was fixed at a value in the range between 1·0 and 0·7. The dependence of the minimal χ_r^2 value on $P_2(\cos\beta_v)$ is shown in figure 2. It can be seen that the χ_r^2 surface possesses a clear minimum at $P_2(\cos\beta_v)$ of 0·81, the value found in the analysis with this parameter unconstrained. The small reduction in the value of χ_r^2 obtained in this way indicates either a small improvement in the quality of the fit over the entire time window or a marked change in the fit across a narrow time interval. We shall show later that the latter case applies here and that the lowering of the χ_r^2 value results solely from marked changes in the fit to a small number of channels directly after the excitation pulse.

Interestingly, we have found that the recovered values of $\langle P_4\rangle$ and $D_\perp$ are particularly sensitive to the value of $P_2(\cos\beta_v)$, this in contrast to $\langle P_2\rangle$, (see figure 3). The values obtained for the three parameters for $P_2(\cos\beta_v) = 1{\cdot}0$ are in fact in excellent agreement with those reported by Straume and Litman [13] for the same vesicle system. Figure 3 shows that $D_\perp$ increases from 0·089 ns^{-1} for $P_2(\cos\beta_v)$ of 0·81

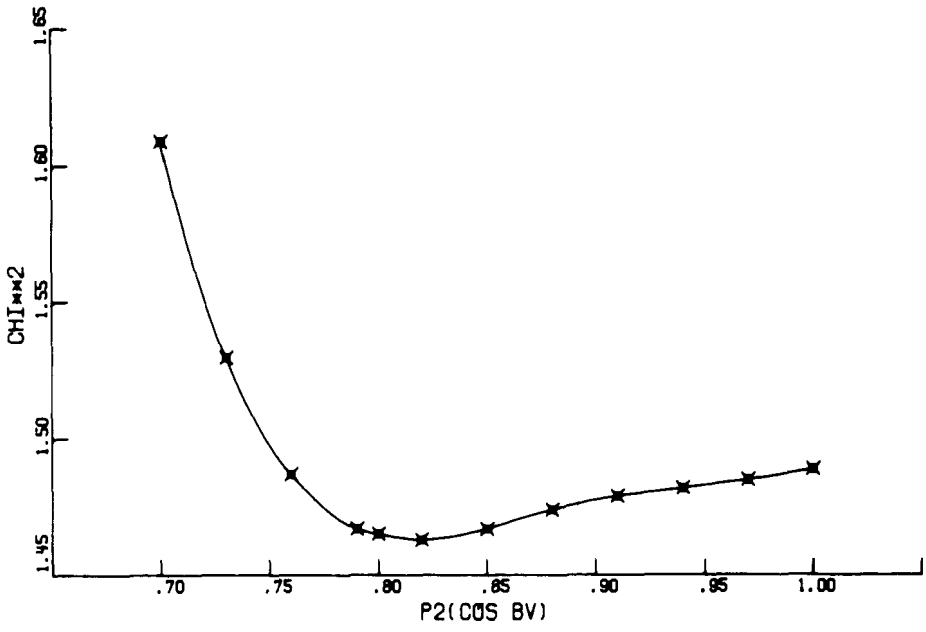

Figure 2. The variation of the minimal χ_r^2 value with $P_2(\cos\beta_v)$ for TMA-DPH in POPC vesicles.

to $0{\cdot}56\,ns^{-1}$ for $P_2(\cos\beta_v)$ of 1·0. The strong dependence of $D_\perp$ on $P_2(\cos\beta_v)$ is also reflected in the individual correlation times $\tau_k = 1/(D_\perp\alpha^k)$ characterizing the mono-exponential decay of the correlation functions $G_k(t)$, (see equation (11)) and shown in figure 4. Remarkably the correlation times τ_1 and τ_2 increase markedly with decreasing values of $P_2(\cos\beta_v)$. For $P_2(\cos\beta_v)$ of 1·0, we find that the correlation functions $G_1(t)$ and $G_2(t)$ decay so rapidly, that they contribute to any significant extent only to the first 10 channels (~ 800 ps). Thus about 40 per cent of the anisotropy amplitude disappears within the first nsec of the decay. The fluorescence anisotropy decay is thus dominated by the correlation function $G_0(t)$. Consequently extrapolation of the long decay component to time zero, will yield a value of $r(0)$ markedly smaller than 0·4. This effect is alleviated considerably on lowering the value of $P_2(\cos\beta_v)$. The decrease in $P_2(\cos\beta_v)$ is effectively compensated by a slower decay of $G_1(t)$ and $G_2(t)$, so that they contribute to the signal at longer times. The minimum in the χ_r^2 surface is thus apparently reached by a trade-off between these two effects. Interestingly, experiments on oriented multibilayers of POPC yield a similar value for $P_2(\cos\beta_v)$ as reported here [9, 17], though the diffusion constant was found to be significantly lower (i.e. longer correlation times τ_k).

It is interesting to note further that the order parameter $\langle P_4\rangle$ is also strongly correlated to $P_2(\cos\beta_v)$ and decreases from 0·55 to 0·42 on decreasing $P_2(\cos\beta_v)$ from 1·0 to 0·81. This change in $\langle P_4\rangle$ implies that the apparent population of TMA-DPH molecules lying with their axes parallel to the plane of the bilayer decreases considerably on lowering the value of $P_2(\cos\beta_v)$. It appears, therefore, that the parameter $P_2(\cos\beta_v)$ determines the detailed interpretation of the experimental data in terms of the molecular orientational order and dynamics of the TMA-DPH molecules. Conse-

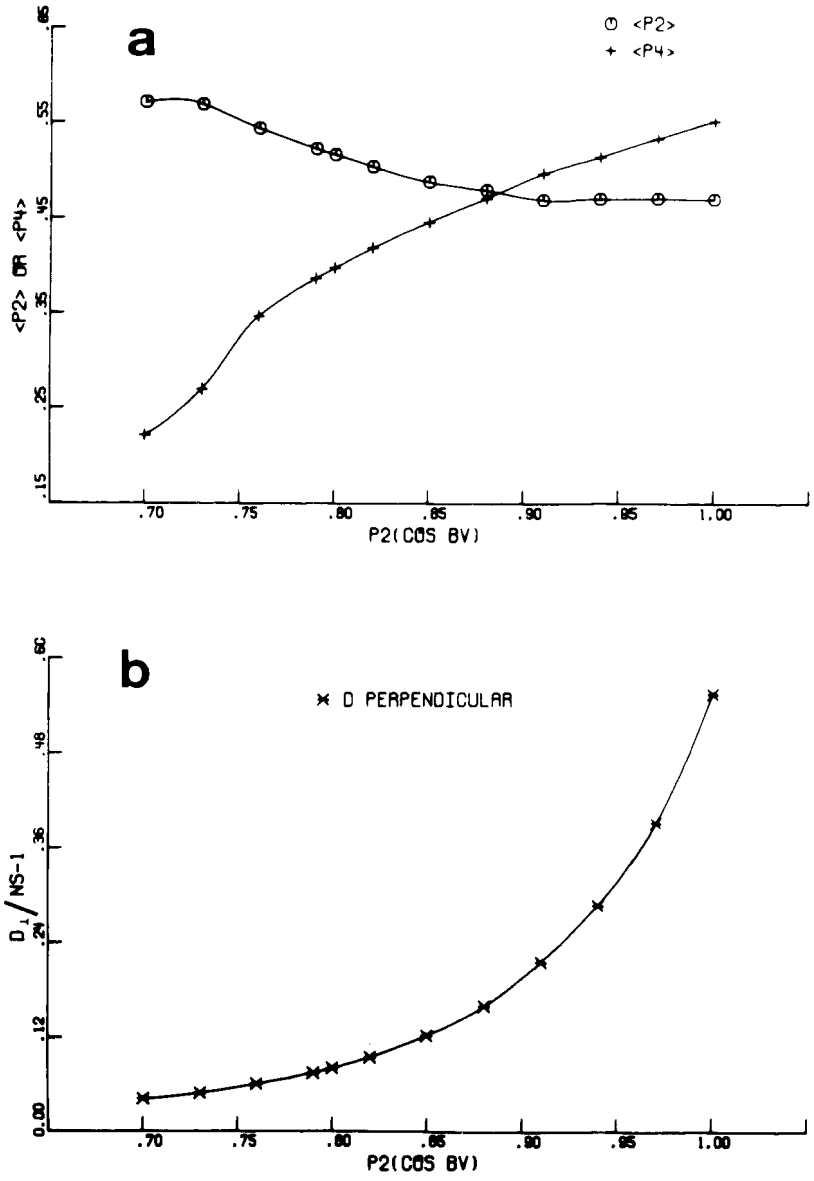

Figure 3. The variation of (*a*) the order parameters $\langle P_2 \rangle$ and $\langle P_4 \rangle$ and (*b*) the diffusion coefficient $D_\perp$ with $P_2(\cos\beta_v)$ for TMA-DPH in POPC vesicles.

quently an injudicious assumption about the orientation of the emission moment relative to the long molecular axis will distort the recovered fit parameters to a large extent. We believe that an objective and unprejudiced fit can only be obtained from analyses in which $P_2(\cos\beta_v)$ is taken to be an adjustable parameter.

This analysis is based on the explicit assumption that the absorption transition moment of TMA-DPH lies along the long molecular axis. The validity of this approach can be tested by fitting the experimental data to the general expression for

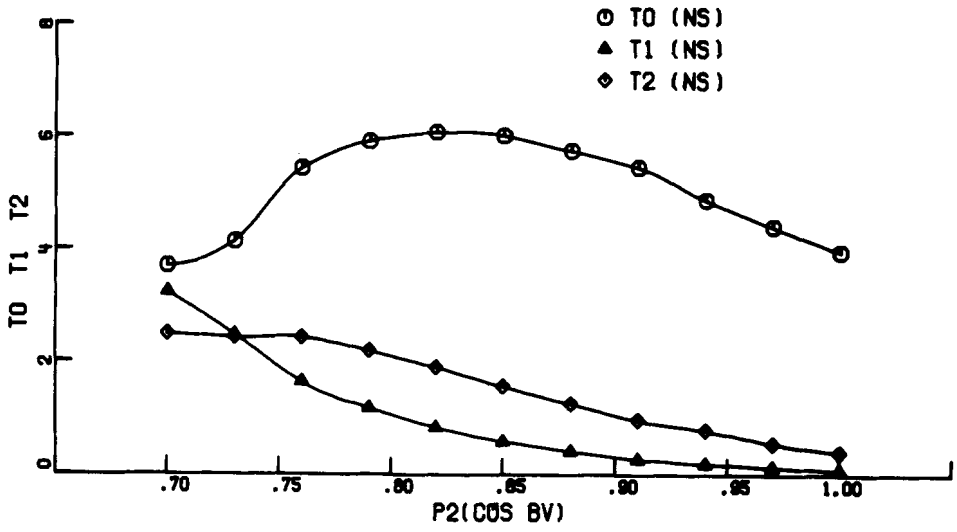

Figure 4. The variation of the correlation times τ_k, $k = 0, 1, 2$ of the correlation functions $G_k(t)$ with $P_2(\cos\beta_v)$.

the anisotropy decay [23] as was previously done by Best *et al.* [25]. Even though we have found $r(0) = 0{\cdot}314$ from a simple multi-exponential analysis of the anisotropy decay, we shall take the two transition moments to be parallel, but tilted by an angle β away from the long molecular axis. The numerical analysis of the data appeared to be flawed in that the optimization procedure first markedly increased the diffusion coefficient around the long molecular axis, $D_\parallel$, before attempting to improve the fit by changing the orientation of the transition moments. This in fact transpires to be a pathological property of the numerical fit to the general expression. Consequently, the anisotropy was found to decay within one channel from a value of 0·4 to 0·32 and the recovered fit parameters were identical to those obtained previously. Although we may assign $\beta = 15°$, we do not believe this to be a satisfactory physical solution in view of the strange decay of the anisotropy and our earlier observations of the differences in the order parameters S_μ and S_v in oriented systems [9, 17].

The question now arises as to whether the potential used in our analysis (see equation (9)) which is symmetric about $\beta_{sm} = \pi/2$ may be used to describe the microscopic behaviour of the TMA-DPH molecules. These molecules are anchored by their polar headgroups at the aqueous interface of the bilayer and are not expected to access orientations with $\beta_{sm} > \pi/2$. We have therefore attempted to fit the data using the simple potential

$$U(\beta_{sm}) = -kT\{\lambda_1 P_1(\cos\beta_{sm}) + \lambda_2 P_2(\cos\beta_{sm})\}, \tag{17}$$

where $P_1(\cos\beta_{sm})$ is $\cos\beta_{sm}$. This potential is symmetric about $\beta_{sm} = \pi$. We expect, however, that this potential will satisfy our requirement for the molecular orientations only if $|\lambda_1| \gg |\lambda_2|$. Now the macroscopic orientational distribution function $f(\beta_{sm})$ is given by

$$f(\beta_{sm}) = N\exp(\lambda_2 P_2(\cos\beta_{sm})\}\,[\exp(\lambda_1\cos\beta_{sm}) + \exp(-\lambda_1\cos\beta_{sm})] \tag{18}$$

as the sign of the odd order parameters is determined simply by the sign of λ_1. Thus

$f(\beta_{sm})$ (see equation (18)) is characterized only by the even order parameters as the odd ones cancel identically. Interestingly the correlation functions $G_k(t)$, (see equation (7)) were found to be invariant to the sign of λ_1 and are thus only determined by the absolute values of the odd order parameters. Unfortunately we have found that the potential, given in equation (17), only spans a very limited region in the $(\langle P_2\rangle, \langle P_4\rangle)$ plane. It appears furthermore to be ill-behaved in that region as there is no unique relation between the parameter pair (λ_1, λ_2) and the order parameter pair $(\langle P_2\rangle, \langle P_4\rangle)$. This is in contrast to our chosen potential given in equation (9). Consequently the fit of the data using this description becomes numerically unstable and we have not been able to obtain a statistically significant solution. An analysis using a more extended potential has not been attempted as more adjustable parameters need now be optimized.

4.2. *DPH in paraffin oil*

In order to test the methodology of time- and angle-resolved fluorescence depolarization experiments on slab-shaped samples, we have carried out two experiments on DPH solutions (5×10^{-6} M) in paraffin oil using different scattering geometries. Firstly, the conventional experiment on a DPH solution in a cuvette was used to determine the time-dependent fluorescence anisotropy, (see equation (15)). Secondly, angle-resolved measurements were carried out on a thin film of a DPH solution, $\sim 400\,\mu$m in thickness, contained between two glass plates. Here the horizontally polarized exciting beam was normally incident on the sample plane and the fluorescence was detected for $\phi = 20°$, 30°, 40° and 50°. All the angles were measured in air outside the sample; the refractive index of paraffin oil was found to be 1·47. The eight observed intensities $I_{HV}(t)$ and $I_{HH}(t)$ were analysed simultaneously using equations (5*c*) and (5*d*) but with $S_\mu = S_v = 0$ and

$$G_0(t) = G_2(t) = (1/5)P_2(\cos\beta_v)\exp(-6D_\perp t).$$

Note that the correlation function $G_1(t)$ is not observed for the geometries chosen. Lifetime measurements indicated that the intrinsic fluorescence decay of the DPH molecules is essentially monoexponential. A biexponential analysis yielded a somewhat better fit, but the additional component contributed less than 10 per cent of the total amplitude. Interestingly, the values of the two parameters $P_2(\cos\beta_v)$ and $D_\parallel$ recovered from the fits were found not to be sensitive to the detailed form of $F(t)$. An example of the fit of the data obtained from a slab-shaped sample is shown in figure 5. The recovered parameters $P_2(\cos\beta_v) = 0{\cdot}804 \pm 0{\cdot}002$. $D_\parallel = 0{\cdot}070 \pm 0{\cdot}002\,\text{ns}^{-1}$ and $\tau_F = 10{\cdot}4 \pm 0{\cdot}2$ ns from the experiments on the slab-shaped samples were in excellent agreement with those obtained from the conventional experiments, $0{\cdot}818 \pm 0{\cdot}002$, $0{\cdot}072 \pm 0{\cdot}002\,\text{ns}^{-1}$ and $10{\cdot}1 \pm 0{\cdot}2$ ns respectively.

4.3. *TMA-DPH in POPC multibilayers*

The four pairs of fluorescence intensities $I_{HV}(t)$ and $I_{HH}(t)$ obtained for normal incidence of the exciting beam were analysed simultaneously using equations (5*c*) and (5*d*). Again the intrinsic fluorescence decay function was taken to have the biexponential form, (see equation (16)). The numerical optimization procedure converged to a single minimal reduced χ^2 value for different starting values of the adjustable parameters. This is in contrast to the analysis of the vesicle data. We note here that the scattering geometries have been chosen so as to eliminate the contribution of the correlation function $G_1(t)$ to the measured signal. An example of the fit of the data

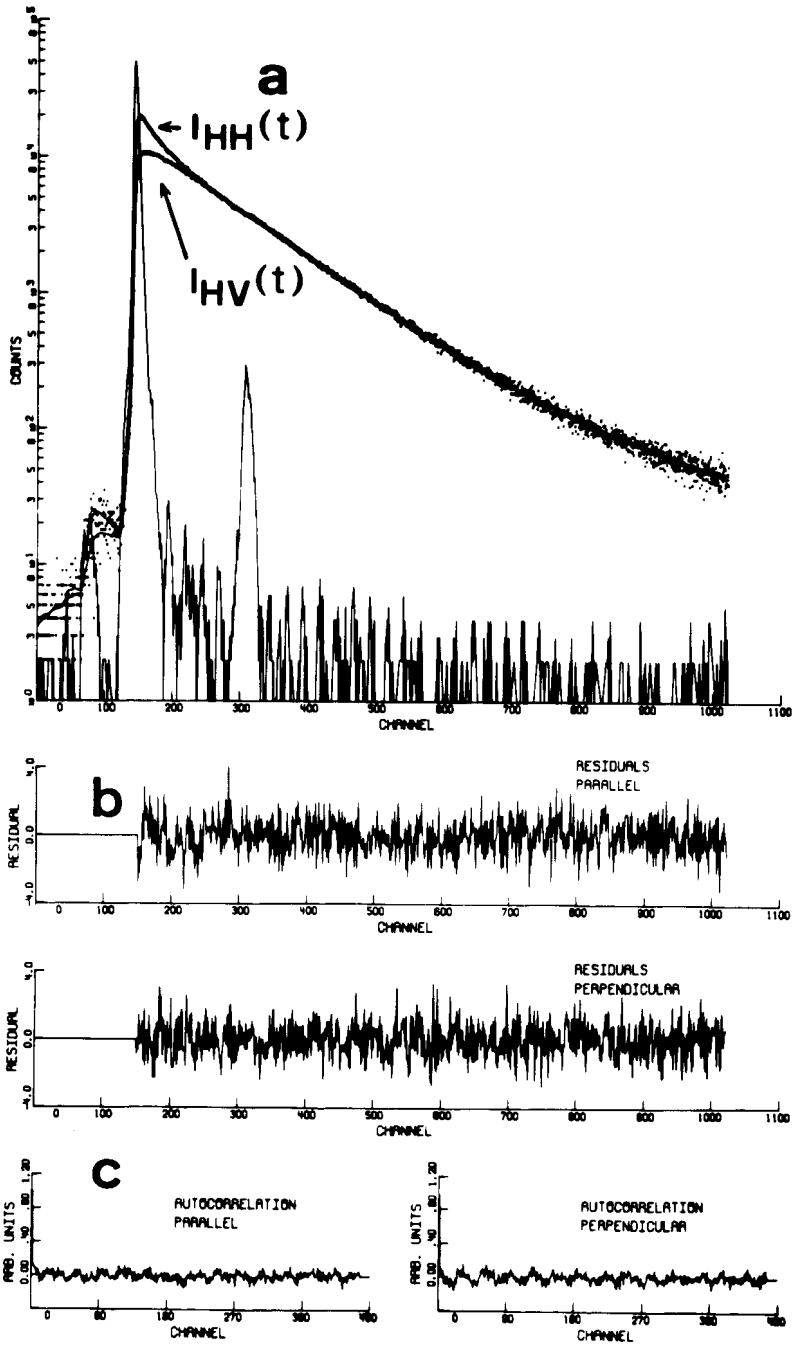

Figure 5. Analysis of the time-resolved signals from a paraffin solution of DPH between glass plates obtained for $\theta = 0$ and $\phi = 30°$. The dots in (*a*) represent the experimental data and the continuous lines give the fit. The excitation pulse profile is also shown. (*b*) The residuals for both components of the fit and (*c*) their autocorrelation function. 1 channel equals 80 ps.

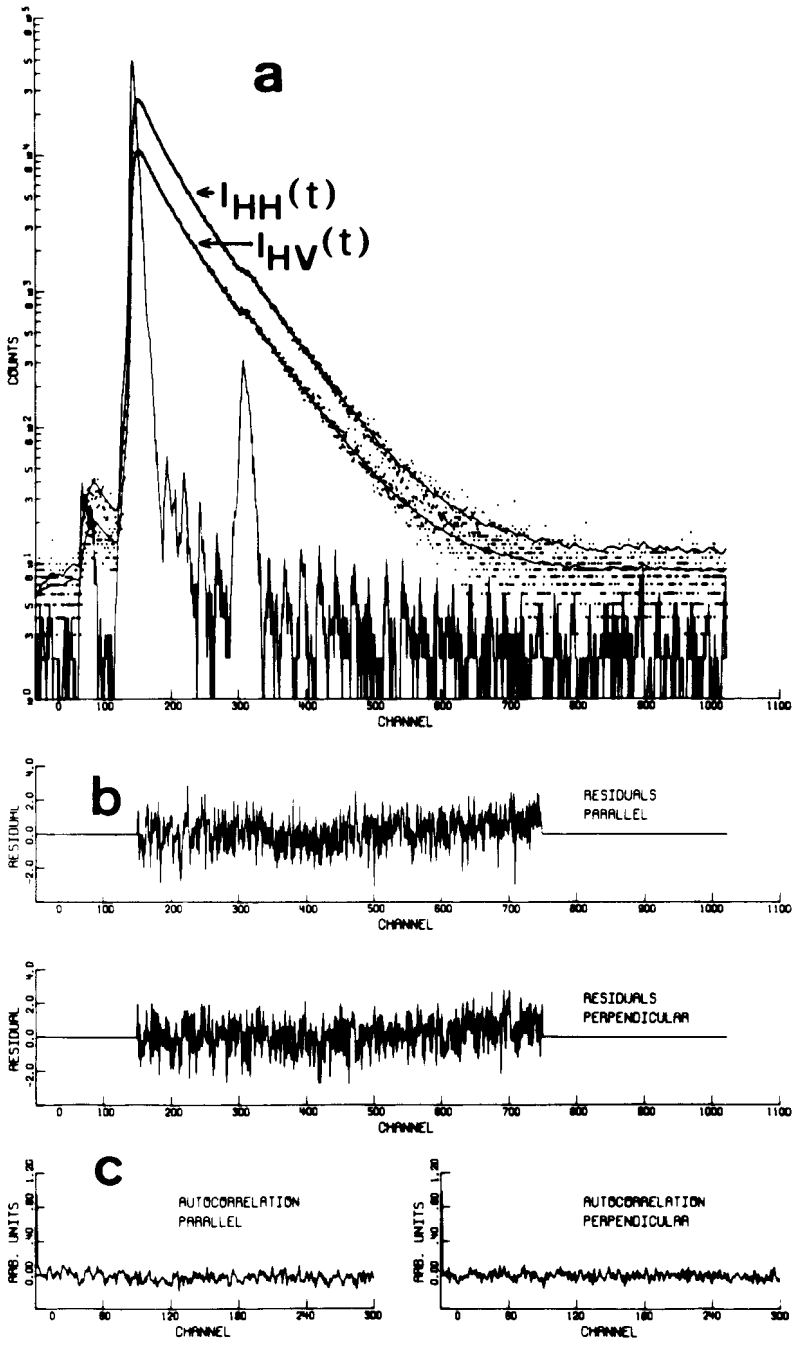

Figure 6. Analysis of the time-resolved signals from TMA-DPH molecules in POPC multibilayers for $\theta = 0$ and $\phi = 50°$. Symbols are as given in figure 5.

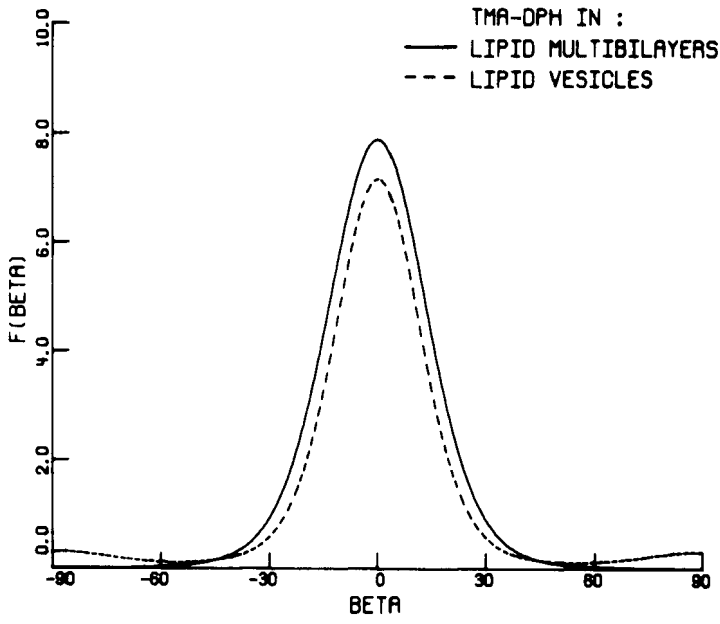

Figure 7. The orientational distribution function of TMA-DPH in slab-shaped multibilayers and spherical vesicles of POPC.

is shown in figure 6; the recovered fit parameters are

$$\begin{aligned}
\beta_1 &= 0{\cdot}222 \pm 0{\cdot}005,\\
\beta_2 &= 0{\cdot}778 \pm 0{\cdot}005,\\
\tau_{F1} &= 1{\cdot}61 \pm 0{\cdot}02\,\text{ns},\\
\tau_{F2} &= 5{\cdot}23 \pm 0{\cdot}02\,\text{ns},\\
\langle P_2\rangle &= 0{\cdot}78 \pm 0{\cdot}02,\\
\langle P_4\rangle &= 0{\cdot}49 \pm 0{\cdot}03,\\
D_\perp &= 0{\cdot}016 \pm 0{\cdot}002\,\text{ns}^{-1},\\
P_2(\cos\beta_v) &= 0{\cdot}81 \pm 0{\cdot}04.
\end{aligned}$$

Again we find that the parameter $P_2(\cos\beta_v)$ is significantly lower than unity, in agreement with the analysis of the vesicle data and our previous results from continuous illumination experiments. Interestingly, the intrinsic fluorescence of the TMA-DPH molecules decays more slowly in multibilayers than in vesicles. The recovered parameters for $F(t)$ found here are in excellent agreement with our earlier determinations of $F(t)$ in planar multibilayers of POPC [9, 17].

It can be seen, from table 2, that the order parameters found for the multibilayers correspond closely only to those given by solution I of the vesicle data. The orientational distribution functions reconstructed from the orienting potentials, (see equation (9)) from these two pairs of order parameters are shown in figure 7. These indicate that the TMA-DPH molecules have a more pronounced tendency to lie parallel to the bilayer surface in the vesicles than in the multibilayer systems. A further striking difference between the planar multibilayer and curved vesicle systems is the

considerably lower diffusion coefficient of the TMA-DPH molecules in the former system.

We believe that our results indicate that the curvature and hydration of the bilayers strongly affects the orientational order and dynamics of the probe molecules.

The authors thank Ms. M. L. Verheijden for the phosphorus determination and Dr. D. Shaw for assistance with the experiments. H.v.L. was supported by the Dutch Foundation for Biophysics under the auspices of the Netherlands organization for Scientific Research (NWO). The use of the SRS was made possible by NWO in connection with the agreement between SERC and NWO.

References

[1] LAKOWICZ, J. R., 1980, *J. biochem. Biophys. Meth.*, **2**, 91.
[2] ZANNONI, C., ARCIONI, A., and CAVATORTA, P., 1983, *Chem. Phys. Lipids*, **32**, 179.
[3] KINOSITA, K., JR., KAWATO, S., and IKEGAMI, A., 1984, *Adv. Biophys.*, **17**, 147.
[4] CRANNEY, M., CUNDALL, R. B., JONES, G. R., RICHARDS, J. T., and THOMAS, E. W., 1983, *Biochim. biophys. Acta*, **735**, 418.
[5] PRENDERGAST, F. G., HAUGLAND, R. P., and CALLAHAN, P. J., 1981, *Biochemistry*, **20**, 7333.
[6] KOOYMAN, R. P. H., VOS, M. H., and LEVINE, Y. K., 1983, *Chem. Phys.*, **81**, 461.
[7] SZABO, A., 1984, *J. chem. Phys.*, **81**, 150.
[8] VANDEVEN, M. J. M., and LEVINE, Y. K., 1984, *Biochim. biophys. Acta*, **777**, 283.
[9] MULDERS, F., VAN LANGEN, H., VAN GINKEL, G., and LEVINE, Y. K., 1986, *Biochim. biophys. Acta*, **859**, 209.
[10] VAN GINKEL, G., KORSTANJE, L. J., VAN LANGEN, H., and LEVINE, Y. K., 1986, *Faraday Discuss. chem. Soc.*, **81**, 49.
[11] CUNDALL, R. B., and DALE, R. E. (editors), 1983, *Time-Resolved Fluorescence Spectroscopy in Biochemistry and Biology* (Plenum Press).
[12] AMELOOT, M., HENDRICKX, HERREMAN, W., POTTEL, H., VAN CAUWELAERT, F., and VAN DER MEER, B. W., 1984, *Biophys. J.*, **46**, 525.
[13] STRAUME, M., and LITMAN, B. J., 1987, *Biochemistry*, **26**, 5113.
[14] VAN LANGEN, H., LEVINE, Y. K., AMELOOT, M., and POTTEL, H., 1987, *Chem. Phys. Lett.*, **140**, 394.
[15] VAN DER MEER, B. W., KOOYMAN, R. P. H., and LEVINE, Y. K., 1981, *Chem. Phys.*, **66**, 39.
[16] VAN LANGEN, H., ENGELEN, D., VAN GINKEL G., and LEVINE, Y. K., 1987, *Chem. Phys. Lett.*, **138**, 99.
[17] DEINUM, G., VAN LANGEN, H., VAN GINKEL, G. and LEVINE, Y. K., 1988, *Biochemistry*, **27**, 852.
[18] JOHANSSON, L. B.-Å., and LINDBLOM, G., 1980, *Q. Rev. Biophys.*, **13**, 63.
[19] ROSE, M. E., 1957, *Elementary Theory of Angular Momentum* (Wiley).
[20] NORDIO, P. L., and SEGRE, U., 1979, *The Molecular Physics of Liquid Crystals*, edited by G. R. Luckhurst and G. W. Gray (Academic Press), Chap. 18.
[21] ZANNONI, C., 1979, *The Molecular Physics of Liquid Crystals*, edited by G. R. Luckhurst and G. W. Gray (Academic Press), Chap. 3.
[22] *The Maximum Entropy Formalism*, 1979, edited by R. D. Levine and M. Tribus (MIT Press).
[23] VAN DER MEER, B. W., POTTEL, H., HERREMAN, W., AMELOOT, M., HENDRICKX, H., and SCHRÖDER, H., 1984, *Biophys. J.*, **46**, 515.
[24] AWAYA, T., 1979, *Nucl. Instrum. Meth.*, **165**, 317.
[25] BEST, L., JOHN, E. and JÄHNIG, F., 1987, *Europ. Biophys. J.*, **15**, 87.
[26] CHEN, P. S. JR., TORIBARA, T. Y., and WARNER, H., 1956, *Analyt Chem.*, **28**, 1756.